Damage reduction of on-board structures using piezoelectric components and active modal control - Application to a printed circuit board

Baptiste Chomette, Simon Chesne, Didier Rémond, Luc Gaudiller

Damage reduction of on-board structures using piezoelectric components and active modal control - Application to a Printed Circuit Board

B. Chomette, S. Chesné, D. Rémond, L. Gaudiller*

Université de Lyon, CNRS

INSA-Lyon, LaMCoS, UMR5259, F-69621, France

Abstract:

The reliability of Printed Circuit Boards (PCB) is critical for on-board electronic systems, particularly when subjected to severe stress conditions. This paper presents an approach to reduce vibration damage in PCBs that can be extended to the majority of on-board structures subjected to damage. Vibration damage highly depends on mode shapes under large band excitations. A solution to reduce vibration from the most damaging modes is to use active modal control for targeting efficiently control energy on most damaging modes. Following this modal-damage strategy, the most damaging modes are determined using a damage analysis based on an initial detailed Finite Element Model (FEM) of the PCB. The control is then designed using only a few piezoelectric components located so as to be essentially effective on these modes. The location algorithm of these active components uses a second simplified FEM including the damage simulation results. Finally, a classical Linear Quadratic Gaussian algorithm is used to determine the modal controller-observer gains.

The effectiveness of the proposed method for PCBs is then examined through experiments with different high level excitations. The proposed control is finally validated by a new damage analysis of the controlled PCB to estimate damage reduction. Based on results obtained on an actual PCB, the modal approach the optimal link between damage estimation, optimal placement of actuators ,optimal control, and minimization of control energy. Moreover, the predictions of damage reduction and of actuation energy are in good agreement with experimental results, what shows that the modal description of on-board smart structure, in particular PCB , is the key point in damage reduction with vibration active control.

Keywords:

Damage analysis; Smart structures; On-board flexible structures; Modal active control; Printed Circuit Boards, Piezoelectricity

1. Introduction

On-board structures are becoming lighter, flexible and they are used in complex and embedded applications. Their flexibility and brittleness have increased and their dynamic behaviour must be controlled early at their design stage. For example, military and aerospace companies must often develop systems that use using commercial Printed Circuit Boards (PCB) in severe operating environments. Moreover, current industrial applications bring about serious difficulties in describing the dynamic behaviour of on-board structures, particularly due to boundary conditions and modelling of actual and complex geometry. In the particular case of on-board PCBs, they are subjected to severe stress conditions like high level broadband vibrations which affect their lifetime, as shown by Starr [1]. Therefore, reduction of damage on such realistic on-board structures needs a specific control strategy which targets damaging modes, using only few actuating components, with minimal actuation energy.

In the `70s and `80s, simple equations such as Steinberg's rule [2] were developed to predict PCB life time. These equations were based on one direction of curvature. However, PCB boundary conditions using standoff, wedge-locks, connectors and frames can be very different from simple clamping. Consequently, curvature can be very complex. As a result, empirical rules were not adapted to industrial PCBs. Zhu, Qu and Wang [3] studied the solder joint fatigue failure mechanism in order to find its main causes. They demonstrated that failures under vibration are typically fatigue failures. Two methods can mainly be applied to understand and predict failures: experiments and Finite Element Analysis (FEA). Li [4] developed a methodology for the fatigue prediction of electronic components under random vibration load based on a detailed FEM of solder joints. The predicted results were validated using experimental observations. Wang and Chai [5] developed an FEM for PCBs, including solder ball modelling, to investigate the effect of drop impact on failure analysis. Nowadays, damage modelling can be considered as mature and integrated in classical FEA approach, but has never been linked to a vibration control on light structures.

There are two main methods for reducing vibration, i.e. vibration isolation applied on the support or vibration control of the PCB. These two methods can be passive or active. In the first case, the isolation system is autonomous and does not need any energy input. For example, in 1970 Veilleux [6] proposed a system based on silicone rubber placed on the PCB support to reduce vibration. Silin, Royzman and Strelbitsky [7] proposed a suspension for PCB with a dry-friction damper. The vibration isolation system can

be active to increase isolation efficiency by using external energy. In case of on-board systems, this energy has to be minimal. Piezoelectric components are particularly adapted for on-board system control. Indeed, they can be easily embedded in electronic systems as actuators or sensors to create a smart structure. These isolation strategies cannot have any effect on mode shapes which mainly affect damage of PCBs and seem to have limited effect in case of broadband and high level excitations.

Several active control strategies can be used such as collocated control as introduced in [8]. In this case, system stability is guaranteed, and what is more, this method does not need a model. Conversely this kind of control cannot be focused on specific modes. Active modal control is a solution for targeting control energy only on specific modes, so on-board amplifier mass and encumbering can be minimized. Few researches have been conducted on light and complex structures like PCB. Though, most of works have presented the active modal control of simple one-dimensional structures like cantilever beams. For example, Bailey and Hubbard [9] studied a distributed piezoelectric-polymer for the active vibration control of a cantilever beam. Modal control permits also to minimize the number of control components [10] Further research has been performed in the case of on-board structures, to reduce the energy consumed by using non linear modal control, as in Gaudiller [11]-[12], or in case of non linear one-dimensional structures using adaptive modal control [13]. Some recent studies have investigated the active control of plates with simple boundary conditions which reduce the mode shape complexity. Shimon, Richer and Hurmuzlu [14] developed an efficient controller for vibration reduction in a fully clamped plate. Qiu, Zhang and Wu [15] studied the active vibration control of a smart flexible cantilever plate, while Sharma, Singh and Sachdeva [16] developed a fuzzy logic controller for the modal control of a plate. From these studies, control components must be optimally located in order to minimize the control energy and to increase efficiency. Hac and Liu [17] proposed a method for sensor and actuator placement in the motion control of flexible structures which is based on Gramians theory. Qiu, Zhang and Wu [15] proposed an optimal localisation applied on a smart flexible cantilever plate. As yet only few researches have focused directly on industrial and complex structures such as PCBs for optimal placement of actuators. Other attempts in active control of PCBs involve active mass damping like in Esser and Huston [18].

From this bibliography synthesis, FEM appears a good way for evaluating damage on PCBsand modal active control using piezoelectric components is well adapted for reducing vibration in on-board structures

with only few active components. However, no study links damage reduction and modal active control of vibration concerning actual on-board structures.

The aim of this study is to control an industrial structure with a minimum of actuation energy independently of its mechanical environment. Active modal control using piezoelectric components is well-adapted, particularly to target the control energy on the natural frequencies and specific mode shapes. This strategy is presented here with an autonomous on-board PCB with complex industrial boundary conditions and different severe operating conditions. This strategy is deeply based on the coupling between damage analysis and active modal control. The aim of this contribution is to show the correct balance in design of active modal control between damage modelling, mechanical equivalent models to take into account piezoelectric components, location optimization and control optimization. In order to demonstrate the validity of the predictive design strategy, practical experiments have been conducted on an actual PCB which presents complex mode shapes.

After this introduction, the second section of this study recalls the basics needed for modelling, with damage estimation, modal mechanical model including electromechanical couplings, active components placement and classical optimal control algorithm. After a brief description of the system studied proposed in section 3, the fourth section presents, step by step, the numerical analysis and simulations introducing damage reduction . Finally, the damage reduction is presented and the effectiveness of the proposed approach is then examined through experimental applications with high excitation levels transmitted by the PCB mounting.

2. Controller design based on damage calculation

2.1. Damage study

The component damage calculation uses Miner's rule [19]. The damage D defined as the sum of incremental damages which is equal to the number of cycles n_i occurring at each cyclic peak stress, divided by the allowable number of cycles N_i at this peak stress level:

$$D = \sum_i \frac{n_i}{N_i} = \sum_i \frac{l_i}{L_i}, \tag{1}$$

where l_i and L_i are respectively the time and the permissible lifetime at the ith stress level. According to Miner's Rule, a failure occurs when $D = 1$. The maximum lead wire stress for each component is used to

define the damage for this component. Lead wire stress is also defined as the sum of the axial stress and the bending stresses from each of two bending moments. This stress is usually the highest at the corner of a solder joint and is calculated using a stress concentration factor.

2.2. Piezoelectric coupling modeling

This study uses a smart structure in order to be independent of boundary conditions. These structures use embedded piezoelectric actuators and sensors. Assuming no damping, the dynamics of a smart structure with piezoelectric actuators and sensors can be written using an FEM formulation:

$$\begin{cases} M\ddot{\delta} + K\delta + K_{\delta vs} = K_{\delta va} v_a \\ K_{vs\delta}\delta + K_{vsvs} v_s = Q_s \end{cases}, \tag{2}$$

where δ represents the mechanical degree of freedom (DOF) vector, v_a and v_s represent the actuators and sensors electric potential DOF vector. M and K are respectively the mass and structural stiffness matrices. $K_{\delta va}$ and $K_{vs\delta}$ are respectively the coupling matrices between the mechanical and electric potential DOF for actuators and sensors. K_{vsvs} is the capacitance matrix for the sensors and Q_s is the electric charge transmitted to the electrodes of the sensors. If the electric potential DOF vector v_a is driven and if the sensors are connected to charge amplifiers, the sensor electrodes are short-circuited and (2) can be rewritten:

$$\begin{cases} M\ddot{\delta} + K\delta = K_{\delta va} g_a v_a^0 \\ g_s K_{vs\delta}\delta = v_s^0 \end{cases}, \tag{3}$$

where g_a and g_s are respectively the voltage amplifier and the charge amplifier gains (see Fig. 9). v_a^0 and v_s^0 are respectively the voltages applied on the actuators and the voltage measured on the charge amplifiers. With the change of variable from physical coordinates δ to modal coordinates q:

$$\delta = \phi q, \tag{4}$$

where ϕ is the modal shape matrix of the smart structure, and assuming uncoupled modes and low viscous damping, (3) can be rewritten as:

$$\begin{cases} \ddot{q} + \mathrm{diag}\left(2\xi_i\omega_i\right)\dot{q} + \mathrm{diag}\left(\omega_i^{\,2}\right)q = \phi^T K_{\delta va} g_a v_a^0 \\ g_s K_{vs\delta}\phi q = v_s^0 \end{cases}, \tag{5}$$

where ω_i and ξ_i are respectively the frequencies in rad/s and the modal damping of the structure (symbol T denotes the transpose matrix). If the modal electromechanical coupling vectors Π^a and Π^s for the actuators and the sensors are defined by:

$$\Pi^a = \phi^T K_{\delta va} \quad \text{and} \quad \left(\Pi^s\right)^T = K_{vs\delta}\phi. \tag{6}$$

then, (5) can be rewritten in the following:

$$\begin{cases} \ddot{q} + \mathrm{diag}\left(2\xi_i\omega_i\right)\dot{q} + \mathrm{diag}\left(\omega_i{}^2\right)q = g_a\Pi^a v_a^0 \\ g_s\left(\Pi^s\right)^T q = v_s^0 \end{cases}. \tag{7}$$

The system transfer function of the smart-structure subjected to external disturbance can be expressed in modal coordinates with a state space form:

$$\begin{cases} \dot{x} = Ax + Bu + Gw \\ y = Cx \end{cases}, \quad x = \begin{bmatrix} \omega q \\ \dot{q} \end{bmatrix}, \quad y = \begin{bmatrix} v_s^0 \end{bmatrix}, \tag{8}$$

where $w(t)$ represents the external disturbance, $u(t)$ the actuator voltage, $x(t)$ is the state vector and $y(t)$ the output vector. A, B and C are the state matrices defined by

$$A = \begin{bmatrix} 0_{n,n} & \mathrm{diag}\left(\omega_i\right) \\ -\mathrm{diag}\left(\omega_i\right) & -\mathrm{diag}\left(2\xi_i\omega_i\right) \end{bmatrix}, \quad B = \begin{bmatrix} 0_{n,1} \\ g_a\Pi_i^a \end{bmatrix}, \quad C = \begin{bmatrix} g_s\Pi_i^s\left(\omega_i\right)^{-1} & 0_{n,n} \end{bmatrix}. \tag{9}$$

where n is the number of modes in the mechanical model.

2.3. Optimal placement of piezoelectric components for damage reduction

The optimal placement of piezoelectric components is a critical part of the controller design because it is directly linked to the controller effectiveness. Indeed, the application of the optimal placement criterion provides a balance between the importance of uncontrolled and controlled modes. This step requires an FEM analysis for complex structures in order to estimate the mode shapes and curvatures. The optimal location is computed using Hac and Liu criterion [17] weighted by average damage values. This criterion is based on Gramians theory. Due to the piezoelectric components duality, actuators or sensors, this algorithm can be explained using controllability or observability Gramians. Controllability Gramians is defined by

$$W_c = \int_0^{\infty} \left(e^{At} B B^T e^{A^T t} \right) dt. \tag{10}$$

The diagonal terms of the Gramians matrix are homogeneous to the total energy. In the case of transient disturbance the criterion is based on the eigenvalues of the Gramians matrix. The multi modal criterion can be written:

$$J = \sum_{i=1}^{2n} D_a^i \lambda_i \left(\prod_{i=1}^{2n} D_a^i \lambda_i \right)^{\frac{1}{2n}}, \tag{11}$$

where λ_i denotes the eigenvalues of the Gramians matrix and n is the number of tested modes. In the proposed method, the modified criterion is weighted here using modal damage vector D_a^i defined by the damage presented in 2.1 for each mode. It represents the modal damage distribution and permits piezoelectric components to be particularly effective on the most damaging modes.

2.4. Controller design

The modal control strategy is chosen in order to actively control the most damaging modes. Moreover, this strategy allows targeting the control energy on the most damaging modes and consequently minimizing the on-board energy. The classical LQG algorithm is used to determine the controller gains and the control $u(t)$ that minimizes the energetic cost functional

$$J = \int_0^{+\infty} \left(x^T Q x + u^T R u \right) dt, \quad Q \geq 0, \quad R > 0, \tag{12}$$

where Q and R are weighting matrices. As the piezoelectric components are already located to be particularly effective on the most damaging modes, and as the state vector includes frequencies, all the coefficients of the weighting matrix Q are equal. The solution to this problem is a linear constant modal gain feedback

$$u = -K\hat{x}, \tag{13}$$

where K is the solution to the LQR problem and $\hat{x}$ is the reconstructed state obtained from the classical Luenberger observer which is designed as

$$\dot{\hat{x}} = A\hat{x} + Bu + L\left(y - C\hat{x}\right), \tag{14}$$

where L is the observer gain.

3. The system studied

The proposed method is here described and applied to an on-board PCB. The system studied, presented in Fig. 1, is a square epoxy plate clamped on the PCB support via three columns, with three electronic components C1, C2 and C3. The characteristics of the system are detailed in Table 1 where the electronic components are located by their lower left corner. The boundary conditions correspond with industrial configurations which are very different from simple clamping. These boundary conditions have great influence on the mode shapes and consequently the entire modal control strategy. Nodal lines for modes 1 to 7 are presented in Fig. 1 and illustrate the complexity of the system studied due to boundary conditions and geometrical complexity. Damage calculation and piezoelectric component placement require fine Finite Element Model and a placement algorithm.

4. Damage reduction: numerical analysis

Due to the complexity of the structure, two FEMs are used here to separate damage calculation and optimal placement. The first one focuses on the electronic components to determine the most damaging modes of the PCB. The second one focuses on the electromechanical coupling to optimally locate the control components. Finally, a new damage analysis including these components is carried out to check if the most damaging modes are globally the same.

4.1. PCB modeling and damage analysis

Assuming slight modification of the mode shapes induced by the control components, the damage calculation is performed without them. This analysis is carried out using CirVibe® and is based on a detailed FEM of the PCB, including the solder joint geometry presented in Fig. 2. This FEM is fit by using the measured damping values presented in Table 2. These measured modal frequencies and damping coefficients stem from a preliminary Operational Modal Analysis of the actual PCB. Numerical CirVibe® frequencies are in good agreement with the measured frequencies, as shown in Table 2.

This analysis provides the damage distribution presented in Fig. 3. The first, third and fourth modes are the most damaging ones with a contribution of 13%, 17% and 64% respectively to the total damage. A slight modification of this damage distribution can be expected with the influence of the piezoelectric components bonded on the PCB. However, these preliminary results are used in the optimal placement algorithm of the piezoelectric components in (11).

The six first modes will be controlled proportionally regarding the calculated damage distribution. As the number of control components is limited on the PCB, only one actuator and two sensors will be bonded on the PCB to control the system. Their location will be calculated using the optimal placement algorithm.

4.2. Smart structure modeling and piezoelectric components optimal placement

Another FEM of the PCB including piezoelectric components is carried out through COMSOL MULTIPHYSICS in order to determine the optimal placement. The proposed algorithm (Hac and Liu [17]) based on Grammians theory is introduced in this software. Moreover, as electronic components are not explicitly modelled, they are also introduced as equivalent elements, as presented in Fig. 4. The equivalent element thickness t_{eq} is the same as that of the PCB t_{card}. The equivalent mass density ρ_{eq} is defined by

$$\rho_{eq} = \rho_{comp} \frac{t_{comp}}{t_{card}} + \rho_{card}, \tag{15}$$

where t_{comp} and ρ_{comp} are respectively the thickness and the mass density of the electronic component and ρ_{card} is the mass density of the PCB. Assuming that the PCB can be locally approximated with a sandwich plate and using the equivalent Allen stiffness [20], the equivalent Young modulus E_{eq} can be obtained from the equivalent stiffness defined by:

$$E_{eq} t_{eq}^3 = E_{card} t_{card}^3 + E_{comp} t_{comp}^3 + E_{solder\ joint} t_{solder\ joint}^3 + E_{comp} t_{comp} d_{comp}^2 + E_{sj} t_{sj} d_{sj}^2, \tag{16}$$

where E_{comp} and E_{card} are respectively the Young modulus of the electronic component and of the PCB, E_{sj} and t_{sj} are the Young modulus and the thickness of the solder joint, d_{comp} is the distance between the neutral axis of the PCB and of the electronic component one. d_{card} is the distance between the neutral axis of the PCB and of the solder joint one. The model includes 8 modes and 76526 DOF. Measured and numerical frequencies can be compared in Table 3 a good agreement between the experiment and simulation. This

model is only used to place the piezoelectric components on the most damaging modes. Consequently, the larger error on the second mode has a low incidence in the proposed approach.

The calculated optimal locations are presented in Fig. 5. Piezoelectric component locations are presented using x and y coordinates in $(O,\vec{x},\vec{y})$. They are located using the lower left corner of the components. These results can be compared with the damage calculation. Indeed, piezoelectric components are more effective in locations with a high curvature, i.e. in a damaging location for electronic components. The piezoelectric components affect PCB stiffness and mass. Consequently, modal shapes and natural frequencies are different from the first PCB and this modification affects the damage analysis. Thus, a new CirVibe® model including the piezoelectric components is formulated with the piezoelectric components models using equivalent mass and stiffness. Obviously, the stiffness and mode shape changes affect the damage calculation. Consequently, a new damage distribution is obtained and presented in Fig. 6. The first, the third and the fourth modes are always the most damaging modes with a contribution of 18%, 37% and 35% of the total damage. Due to the optimal location, the damage is more distributed on the different modes. The damage contribution of the most damaging mode decreases whereas it increases for the less damaging ones.

4.3. Controller and observer computation for damage reduction: numerical simulations

The control is designed and tested in simulations using the FRF of the uncontrolled (17) and controlled system (18) in modal coordinates, obtained by (8), (13) and (14):

$$H_{nc}(j\omega) = C(j\omega \times Id - A)^{-1} G, \tag{17}$$

$$H_c(j\omega) = C\left(j\omega \times Id - \left(A - BK\left(j\omega \times Id - (A - BK - LC)\right)^{-1} LC\right)\right)^{-1} G, \tag{18}$$

where the system (A,B,C,D) is defined for one actuator and two sensors and for $n = 8$ modes:

$$A = \begin{bmatrix} 0_{n,n} & \mathrm{diag}(\omega_i) \\ -\mathrm{diag}(\omega_i) & -\mathrm{diag}(2\xi_i\omega_i) \end{bmatrix}, B = \begin{bmatrix} 0_{n,1} \\ g_a\Pi_i^a \end{bmatrix}, C = \begin{bmatrix} g_s\Pi_i^{s1}(\omega_i)^{-1} & 0_{n,n} \\ g_s\Pi_i^{s2}(\omega_i)^{-1} & 0_{n,n} \end{bmatrix}, D = \begin{bmatrix} 0 \\ 0 \end{bmatrix}. \tag{19}$$

Control and observation gains are computed in MATLAB using the classical LQ control and observation routines. The maximal control gain values are applied on the third and fourth mode. The distribution vector of the disturbance G assigns the external excitations transmitted by the columns to the modal state X as boundary conditions. The matrix A is obtained from Operational Modal Analysis and curve fitting method.

Matrices B, C and G are obtained by model fitting. The FRF of the controlled system is presented in Fig. 7. The predicted reductions for the modes 3 and 4 are about –8 dB and –17 dB respectively. The modal control voltages in transient and steady state are presented in Fig. 8. They are maximal for the third and the fourth modes. In the first case, the control voltage represents the voltage impulse at the beginning of the control. In the second case, the control voltage represents the voltage when the system is controlled and stabilized. The predicted control voltage is close to 55 V under a 1 g_{rms} disturbance and about 275 V under 5 g_{rms} disturbance.

5. Experimental application

5.1. Experimental setup

The experimental system is presented in Fig. 9. The PCB support is clamped on the shaker platform. Consequently, the white noise disturbance imposed by acceleration tracking is directly transmitted to the PCB by the three columns as in its industrial configuration. The PCB is instrumented with one piezoelectric actuator and two piezoelectric sensors bounded under the PCB. The PCB strains induce electric charges on the electrodes of the two sensors. Consequently, they are connected to a charge divisor in order to measure a voltage proportional to the PCB strain. The piezoelectric actuator is connected to a voltage amplifier. The input and the outputs of the plant are connected to a microprocessor (Dspace 1006 using digitalized signals at $1e^{-4}$s) which calculates the control voltage applied on the actuator using the sensor responses. A reference accelerometer is bonded on the shaker platform to drive the shaker. The experimental equipment is described in Table 4.

5.2. Experimental results

The measured results and modal control voltage obtained under a 1 g_{rms} disturbance are presented in Fig. 10 and in Fig. 11. The simulated study has predicted a -8 dB and -17 dB reduction on the third and fourth modes respectively. Experimentally, the measured FRF shows that the two modes are respectively reduced by -8 and -15 dB. Consequently, there is good agreement between the simulation and the experiments and the damage reduction predicted in the simulation is globally observed experimentally. The damping of these two modes is increased by a factor of 2 and 6 respectively. This amount of damping will lead to damage reduction on the electronic components. Nevertheless, the modal control voltage is less distributed on the damaging modes, as

predicted in the simulation. The measured results and modal control voltage obtained under a 5 g_{rms} disturbance are presented in Fig. 12 and in Fig. 13. The third and fourth modes are reduced by -8 and -11 dB respectively. The clamping behaviour evolves for very high excitation levels (5 to 10 g_{rms}). Consequently, the model used in the controller becomes inaccurate for these levels, leading to a decrease of the controller's performances.

The maximal control voltage is about 79V for 1 g_{rms} and 391V for 5 g_{rms} disturbance. These values show that the control voltage predicted in simulation was a good approximation.

5.3. Damage reduction induced by the control

A new damage analysis is performed to show the damage reduction induced by the active control. Damping values of the controlled system are included as virtual accelerometers located on the PCB model to take into account the action of control on the damage calculation. The new damage distribution is presented in Fig. 14. The damage of the controlled system is more distributed on each mode at lower levels, as shown in Fig. 16. The total damage of the three components, presented in Fig. 15, is reduced by factors of 11 and 181 for the third and fourth mode respectively. Consequently, the life time of the PCB will be increased with the same factor.

The active control supplies a substantial amount of damping to the system, particularly on the third and on the fourth modes. Consequently, the damage caused by these two modes is reduced for the three components. The structure modifications due to the piezoelectric components generally lead to damage reduction except for the first component on the third mode which becomes more damaging. Nevertheless, the damage level for this component is much lower than those of the third component. When comparing the damage of the PCB without piezoelectric components to the damage of the controlled one with piezoelectric components, the damage induced by the third mode is reduced by factors of 7, 43 and 8 for the first, second and third components respectively. The damage caused by the fourth mode is finally reduced by factors of 211, 255 and 181 for the first, second and third components respectively.

6. Conclusion

The aim of this paper is to present the damage reduction of on-board flexible structures subjected to high level disturbances. The method proposed herein is based on modal active control using few piezoelectric components for actuators and sensors. The proposed strategy links damage estimation before control, optimal placement of actuators, optimal control, and minimization of control energy in a well adapted design. The methodology uses a specific PCB for illustrating the benefits of the modal description. Indeed, damage reduction in PCBs is a major challenge for particular industrial configurations. The methodology used by the proposed control design is based on a damage analysis of the PCB to determine the most damaging modes. Due to the complex mode shapes of the system studied, this analysis is performed using a detailed FEM of the PCB including solder joint geometry. Piezoelectric components are then located using an optimal placement algorithm. The most damaging modes are considerably weighted due to damage balance. Consequently, piezoelectric components bounded in these optimal locations are particularly effective on the most damaging modes.

This optimal placement is a critical part of controller design and represents a first part of the control which leads to damage reduction only by the modification of the structure, stiffness and mass, induced by the addition of piezoelectric components. It could be considered as a passive control that permits damage reduction when the active control becomes ineffective. The chosen control strategy is modal in order to target the control energy on the most damaging modes, thus reducing mass and bulk of the amplifier. The experimental results obtained on the PCB show good agreement with the simulation particularly for the vibration reduction but less regarding the control energy distribution. The damage reduction induced by the control is finally calculated using a final damage analysis of the PCB including the damping induced by the control. Both modifications of the structure induced by the piezoelectric components in their optimal location and damping introduced by the modal control permit reducing the damage on each electronic component and consequently increasing the lifetime of the PCB.

The control strategy chosen, i.e. active modal damping instead of isolation, permits reducing on-board external control energy and therefore the amplifier mass and encumbering which is an actual problem for on-board structures. The method designed shows the interaction between piezoelectric components location and control characteristics optimization, in order to target the control energy only on the most damaging modes.

This study demonstrates the efficiency of active modal control in increasing the lifetime of industrial structures. For maintaining the effectiveness of the control at high excitation levels in spite of system nonlinearities, an adaptive control could be developed, particularly by updating the modal parameters. It could be evenly a way to increase the controller robustness in case of mass production with great dispersions or in case of environment variations like boundary conditions, vibration levels or temperature variations.

Acknowledgments:

This study was supported by MBDA France and the CNRS. The authors wish to thank particularly P. Dessendier and R. Sudant from MBDA for their many helpful discussions.

References:

[1] J.E. Starr, W. Tustin, What result from Vibrating electronic Systems, COTS Journal, Test & Screening, Vibration & Shock (2002) 39-42.

[2] S. Steinberg, Vibration Analysis for Electronic Equipment, 2nd Edition, Wiley, New York, 1988.

[3] X. Zhu, B. Qu, J. Wang, Mechanical Test and Analysis on Reliability of Lead-free BGA Assembly, in: IEEE 2005 6th International Conference on Electronic Packaging Technology, pp. 498-502.

[4] R.S. Li, A methodology for fatigue prediction of electronic components under random vibration load. ASME: Journal of Electronic Packaging 123 (2001) 394–400.

[5] Y.Y. Wang, F. Wang, T.C. Chai, Finite element modeling of CSP package subjected to board level drop test. In: Proc 6th electronics packaging technology conference, Singapore, 2004. pp. 684–8.

[6] E.D. Veilleux, Vibration Control of Printed-Circuit Boards in a Dynamic Environment, in: IEEE Transaction on Parts, Materials, and Packaging, vol. PMP-6, No. 3, September 1970, pp. 100-105.

[7] R. Silin, V. Royzman, V. Strelbitsky, Theory and practice of vibro-insulation of printed circuit boards on fabric hanger with dry friction damper, in: 12th IFToMM World Congress, Besançon (France), June18-21, 2007.

[8] A. Preumont, Vibration Control of Active Structures: An introduction, second ed., Kluwer Academic, Dordrecht, 2002.

[9] T. Bailey, J.E. Hubbard, Distributed piezoelectric-polymer active vibration control of a cantilever beam, Journal of Guidance Control and Dynamics 16 (1993) 801-821.

[10] L. Gaudiller, J. Der Hagopian, Active control of flexible structures using a minimum number of components, Journal of Sound and Vibration 193 (1996) 713-741.

[11] L. Gaudiller, F. Matichard, A Nonlinear method for improving the active control efficiency of smart structures subjected to rigid body motions, IEEE/ASME Transaction of Mechatronics 12 (5) (2007) 542-548.

[12] F. Matichard, L. Gaudiller, Improvement of Potential Energetic Exchange Using Nonlinear Control, in: proceedings of IEEE/ASME Advanced Intelligent Mechatronics, California, Monterey, USA, 2005, pp. 807-812.

[13] L. Gaudiller, S. Bochard, "Adaptive active control of flexible structures subjected to rigid body displacements", Journal of Sound and Vibration 283 (2005) 311-339.

[14] P. Shimon, E. Richer, Y. Hurmuzlu, Theoretical and experimental study of efficient control of vibrations in clamped square plate, Journal of Sound and Vibration 282 (2005) 453-473.

[15] Z. Qiu, X. Zhang, H. Wu, H. Zhang, Optimal placement and active vibration control for piezoelectric smart flexible cantilever plate, Journal of Sound and Vibration 301 (2007) 521-543.

[16] M. Sharma, S.P. Singh, B.L. Sachdeva, Modal control of a plate using a fuzzy logic controller, Smart Materials and Structures 16 (2007) 1331-1341.

[17] A. Hac, L. Liu, Sensor and actuator location in motion control of flexible structures, Journal of Sound and Vibration 167 (1993) 239-261.

[18] B. Esser, D. Huston, Active mass damping of electronic circuits boards, Journal of Sound and Vibration 277 (2004) 419-428.

[19] M. A. Miner, Cumulative damage in fatigue, Journal of Applied Mechanics 12 (1945) A159–A164.

[20] Howard. G. Allen**,** «Analysis and design of structural sandwich panels ", Pergamon Press, Oxford, New-york, 1969.

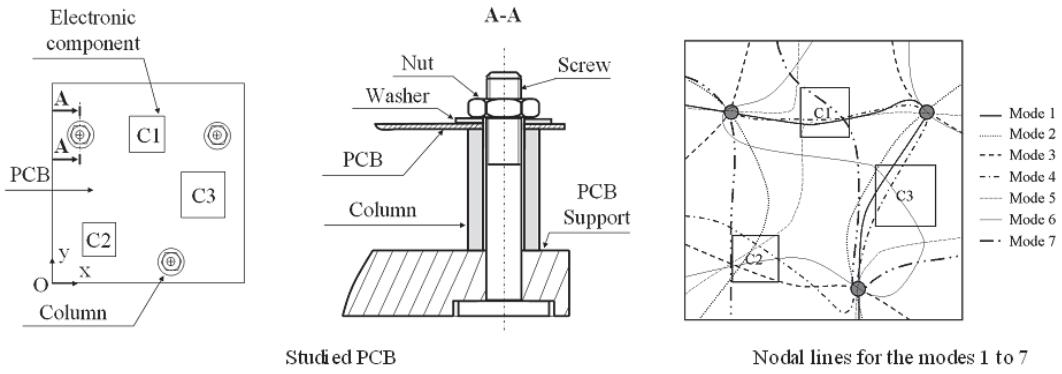

Fig. 1. The system studied

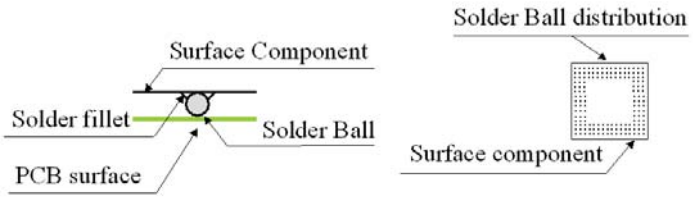

Fig. 2. Component connection geometry.

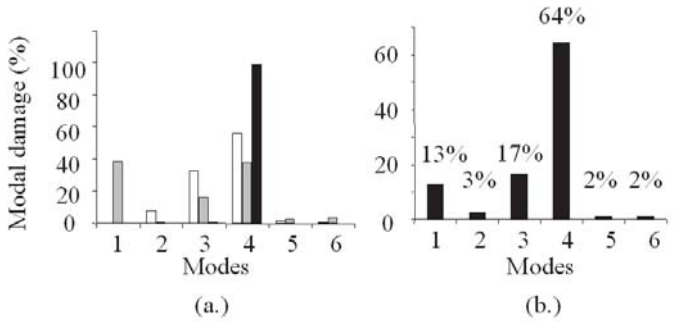

Fig. 3. Damage distribution without piezoelectric components (a.)
(□ component 1, ■ component 2, ■ component 3) and average damage (b.) (■ average damage).

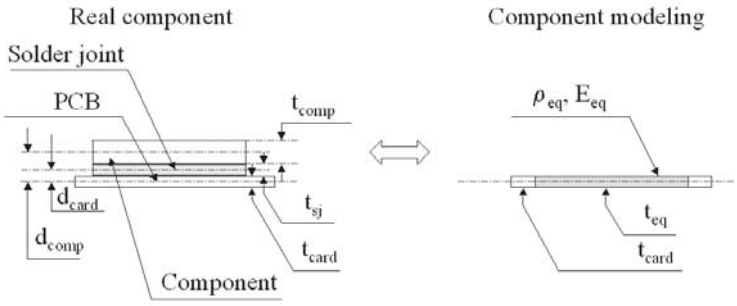

Fig. 4. Component modelling.

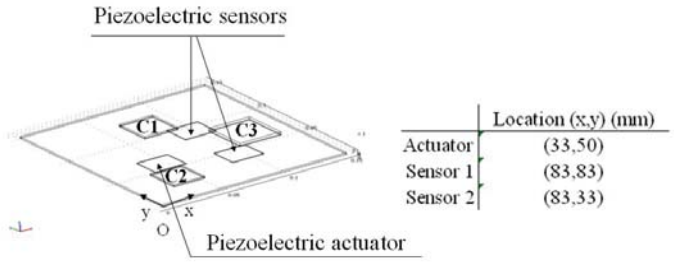

Fig. 5. Optimal location.

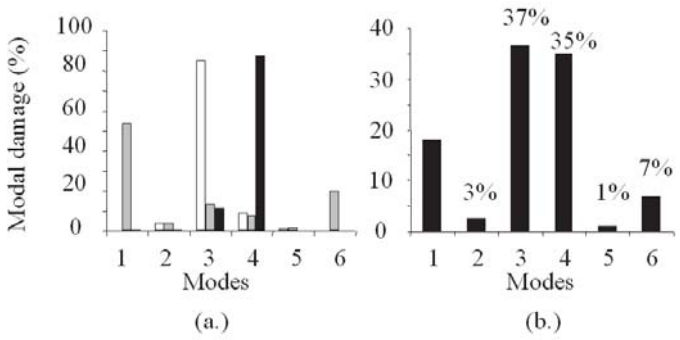

Fig. 6. Damage distribution with piezoelectric components
(a.) (□ component 1, ■ component 2, ■ component 3) and average damage (b.) (■ average damage).

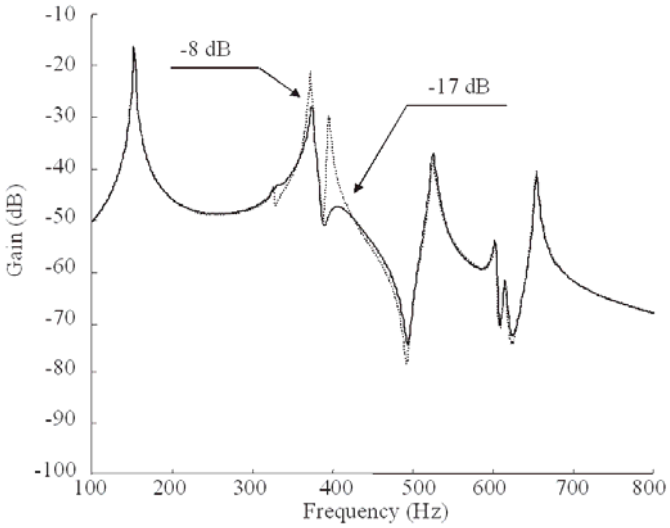

Fig. 7. Numerical uncontrolled (····) and controlled (—) FRF between the accelerometer and the first piezoelectric sensor.

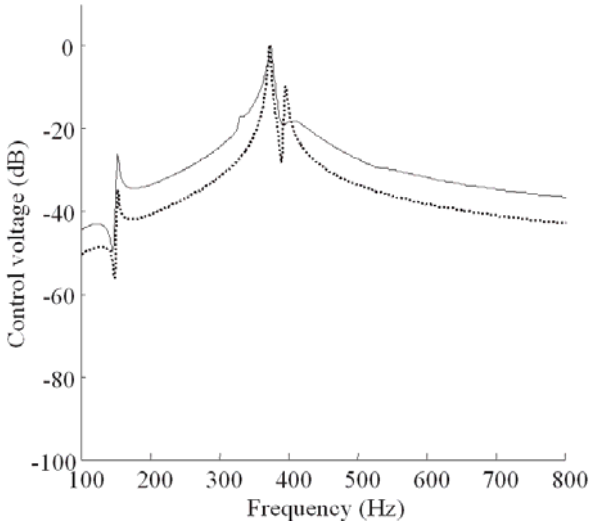

Fig. 8. Numerical control voltage, permanent (—) and transient (····) state.

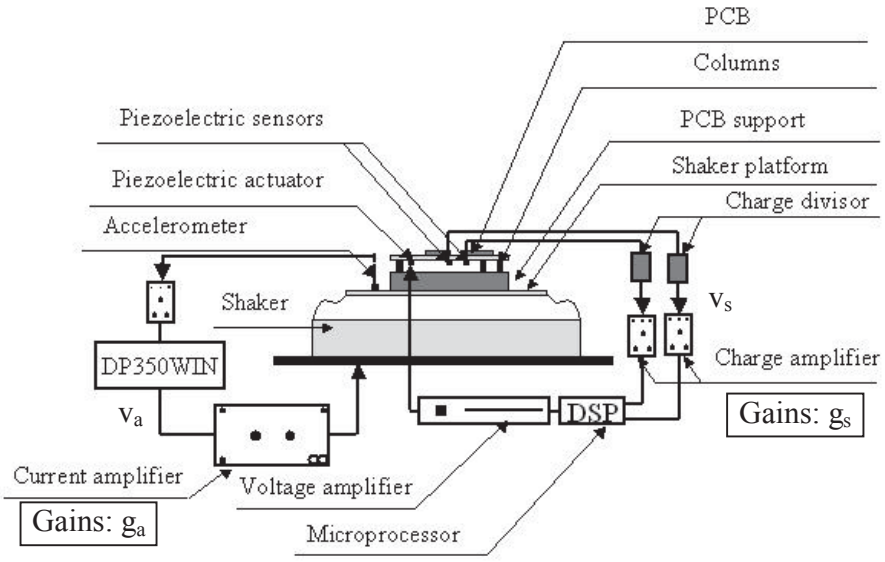

Fig. 9. Experimental set-up.

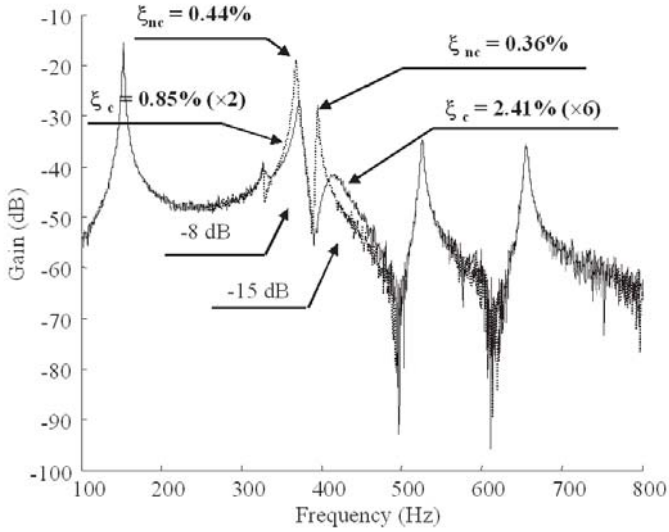

Fig. 10. Experimental uncontrolled (····) and controlled (—) FRF between the accelerometer and the first piezoelectric sensor for a 1 g_{rms} disturbance.

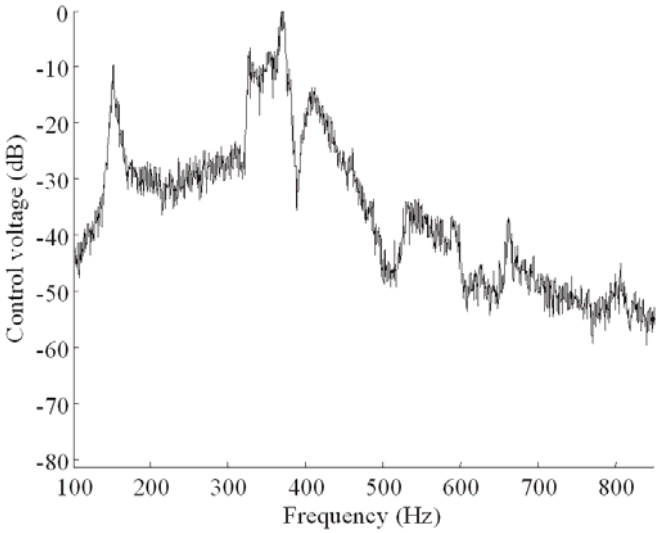

Fig. 11. Modal control voltage for a 1 g_{rms} disturbance.

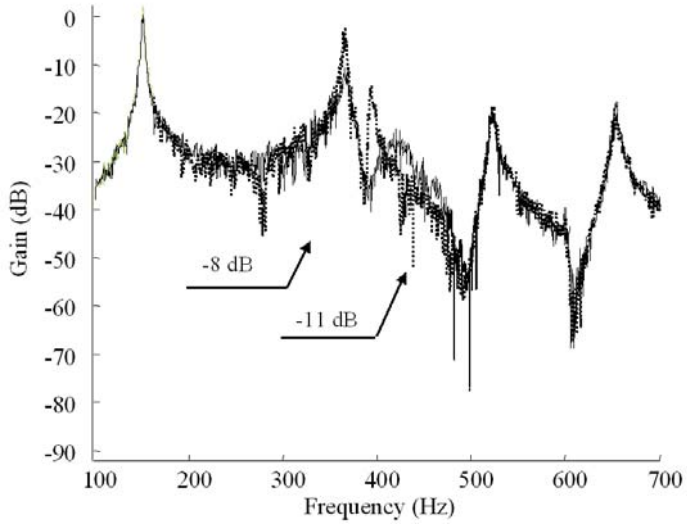

Fig. 12. Experimental uncontrolled (····) and controlled (—) FRF between the accelerometer and the first piezoelectric sensor for a 5 g_{rms} disturbance.

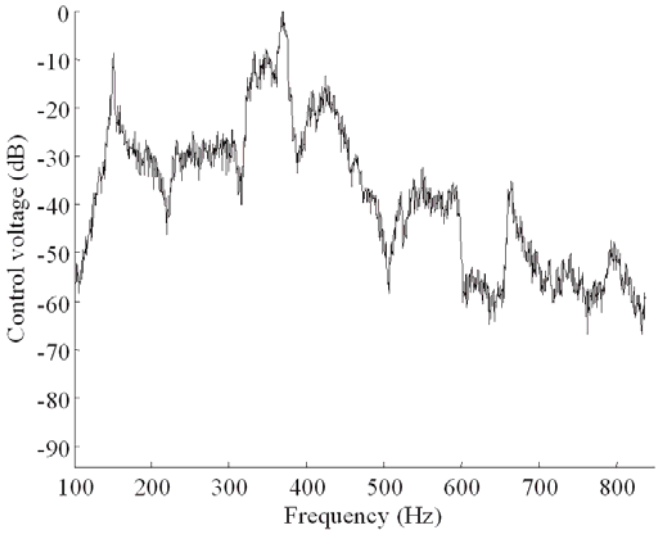

Fig. 13. Modal control voltage for a 5 g_{rms} disturbance.

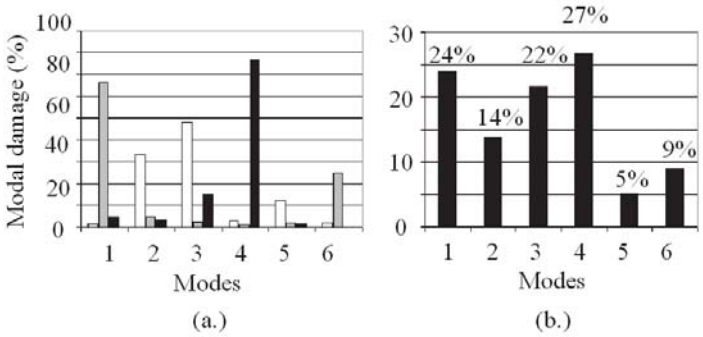

Fig. 14. Damage distribution with piezoelectric components and LQG control.
(a.) (□ component 1, ■ component 2, ■ component 3) and average damage (b.) (■ average damage).

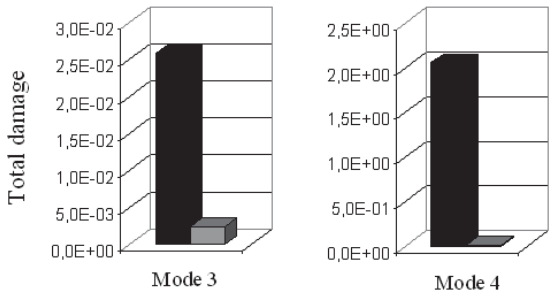

Fig. 15. Total damage reduction on the PCB (■ uncontrolled PCB without piezoelectric components, ■ controlled PCB with activated piezoelectric components).

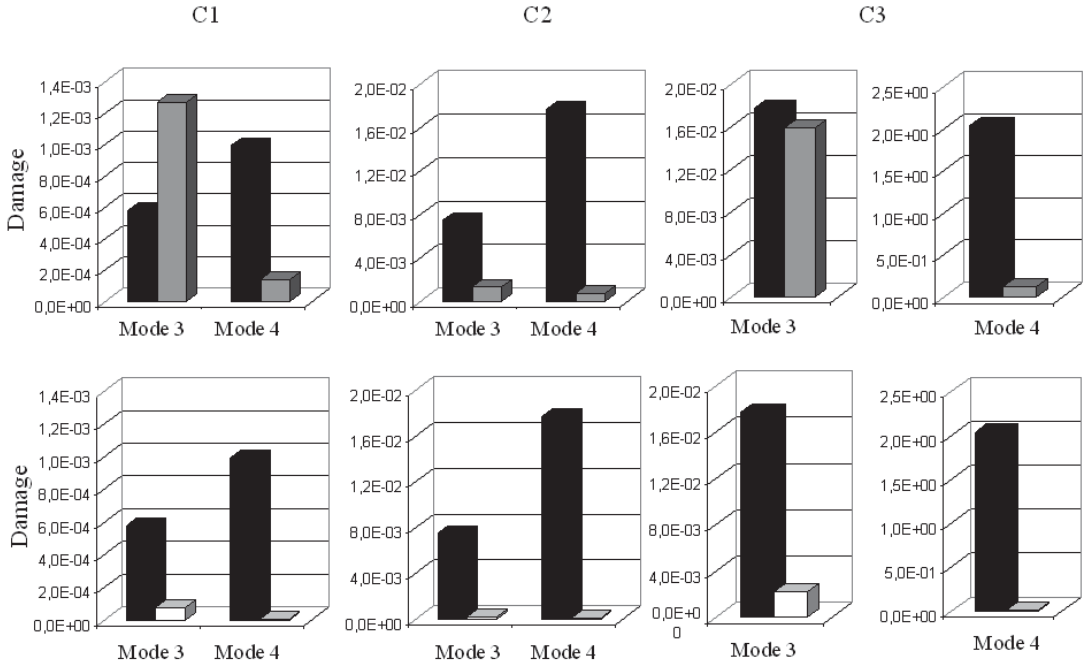

Fig. 16. Damage reduction with LQG control calculated with CirVibe® (■ uncontrolled PCB without piezoelectric components, ■ controlled PCB with activated piezoelectric components).

Table 1: System characteristics

Component	Type	Geometry	Location (x;y) (mm)
C1	bga10K200	27 × 27	(61.4;97.9)
C2	cbga	25 × 25	(25.3; 20)
C3	bga1020	33 × 33	(102.1;50.1)
PCB		Column location (x ; y) (mm)	
Geometry	150 × 150 × 1.62 mm	Column 1	(93;16)
Elastic modulus	19996 MPa	Column 2	(22;111.5)
Mass density	1783 Kg/m^3	Column 3	(129;111.5)

Table 2: Measured and numerical modal parameters

Measured frequencies	CirVibe® frequencies (Hz)	Error	Measured damping (%)
142	150	6%	0.67
310	279	-10%	0.47
358	348	-3%	0.41
372	367	-1%	0.41
454	501	10%	0.3
635	588	-7%	0.3

Table 3: Measured and numerical frequencies

Experimental frequencies (Hz)	Comsol frequencies (Hz)	Error
142	135	-5%
310	241	-22%
358	354	-1%
372	380	2%
454	494	9%
635	669	5%

Table 4: Experimental equipment

Element	Experimental equipment
Shaker	4600N, Gearing & Watson GWV617
Shaker drive software	DP350Win
Piezoelectric components	Piezoelectric ceramic P188
Actuator voltage amplifier	HVPZT-POWER-AMPLIFIER PI
Sensor charge amplifier	B&K 2626
Control system	MATLAB/Simulink/dSpace
Accelerometer	Endevco DQ58 type 5001
Accelerometer charge amplifier	KIAG SWISS type 5001

For following .tiff files of figures and tables:

Figure captions

Fig. 1 : System studied

Fig 2 : Component connection geometry

Fig 3 : Damage distribution without piezoelectric components

Fig 4 : Component modeling

Fig 5 : Optimal location

Fig 6 : Damage distribution with piezoelectric components

Fig 7 : Numerical uncontrolled and controlled FRF between the accelerometer and the first piezoelectric sensor

Fig 8 : Numerical control voltage.

Fig 9 : Experimental set-up

Fig 10 : Experimental uncontrolled and controlled FRF between the accelerometer and the first piezoelectric sensor for a 1 grms disturbance.

Fig 11 : Modal control voltage for a 1 grms disturbance.

Fig 12 : Experimental uncontrolled and controlled FRF between the accelerometer and the first piezoelectric sensor for a 5 grms disturbance.

Fig 13 : Modal control voltage for a 5 grms disturbance.

Fig 14 : Damage distribution with piezoelectric components and LQG control

Fig 15 : Total damage reduction on the PCB

Fig 16 : Damage reduction with LQG control calculated with CirVibe®.

Table captions

Table 1 : System characteristics

Table 2 : Measured and numerical modal parameters

Table 3 : Measured and numerical frequencies

Table 4 : Experimental equipment

Table1: System characteristics
Click here to download high resolution image

Component	Type	Geometry	Location (x;y) (mm)
C1	bga10K200	27 × 27	(61.4;97.9)
C2	cbga	25 × 25	(25.3; 20)
C3	bga1020	33 × 33	(102.1;50.1)
PCB		Column location (x ; y) (mm)	
Geometry	150 × 150 × 1.62 mm	Column 1	(93;16)
Elastic modulus	19996 MPa	Column 2	(22;111.5)
Mass density	1783 Kg/m^3	Column 3	(129;111.5)

Table2: Measured and numerical modal parameters
Click here to download high resolution image

Measured frequencies	CirVibe® frequencies (Hz)	Error	Measured damping (%)
142	150	6%	0.67
310	279	-10%	0.47
358	348	-3%	0.41
372	367	-1%	0.41
454	501	10%	0.3
635	588	-7%	0.3

Table3: Measured and numerical frequencies
Click here to download high resolution image

Experimental frequencies (Hz)	Comsol frequencies (Hz)	Error
142	135	-5%
310	241	-22%
358	354	-1%
372	380	2%
454	494	9%
635	669	5%

Table4: Experimental equipment
Click here to download high resolution image

Element	Experimental equipment
Shaker	4600N, Gearing & Watson GWV617
Shaker drive software	DP350Win
Piezoelectric components	Piezoelectric ceramic P188
Actuator voltage amplifier	HVPZT-POWER-AMPLIFIER PI
Sensor charge amplifier	B&K 2626
Control system	MATLAB/Simulink/dSpace
Accelerometer	Endevco DQ58 type 5001
Accelerometer charge amplifier	KIAG SWISS type 5001

Figure 1 : System studied
Click here to download high resolution image

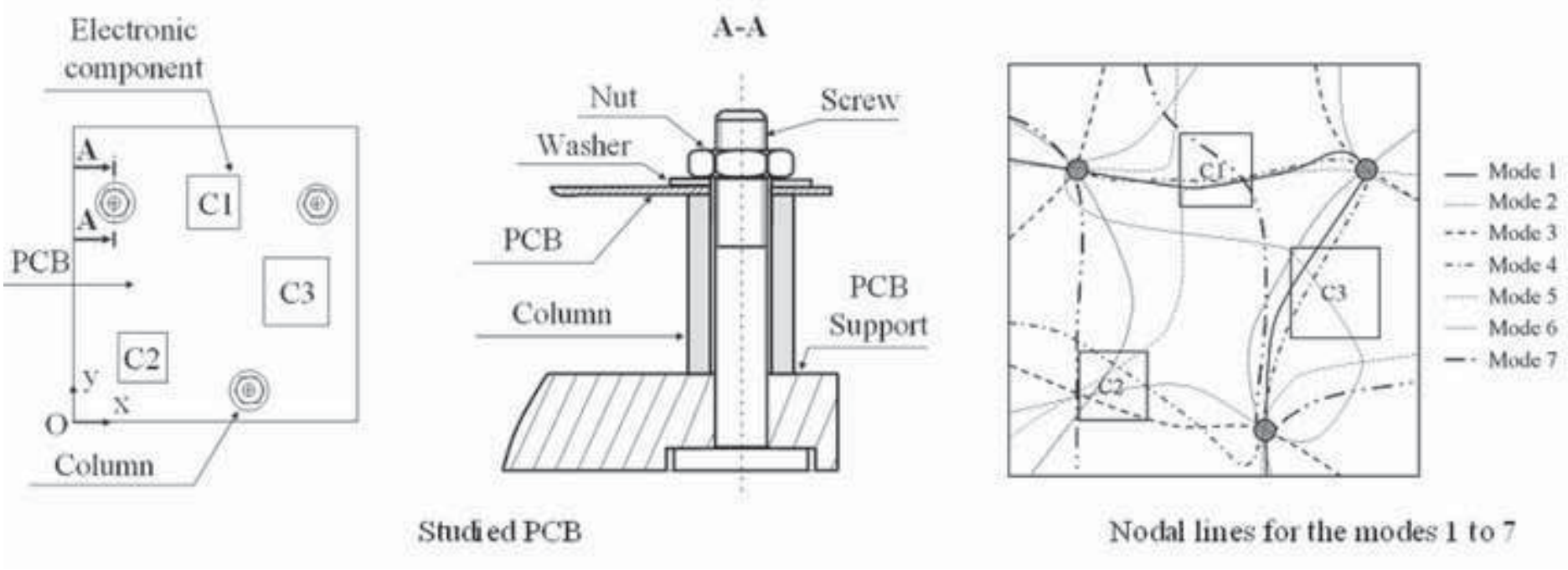

Fig. 2: Component connection geometry
Click here to download high resolution image

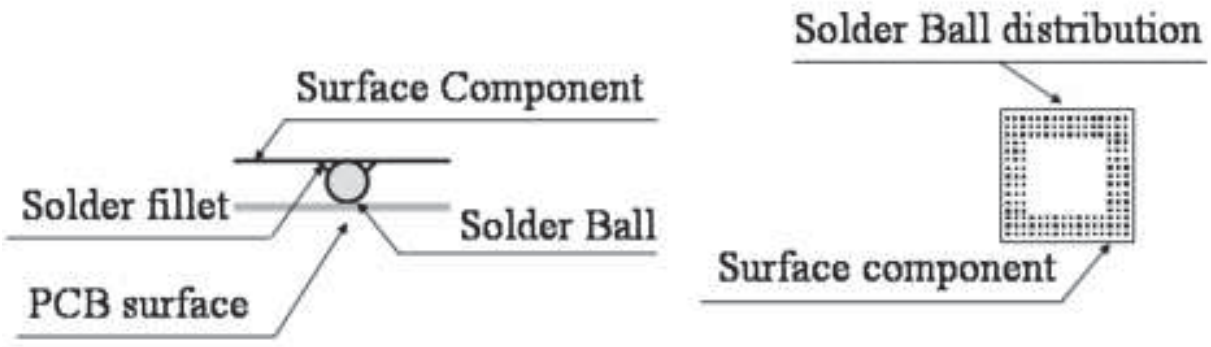

Fig. 3: Damage distribution without piezoelectric components
Click here to download high resolution image

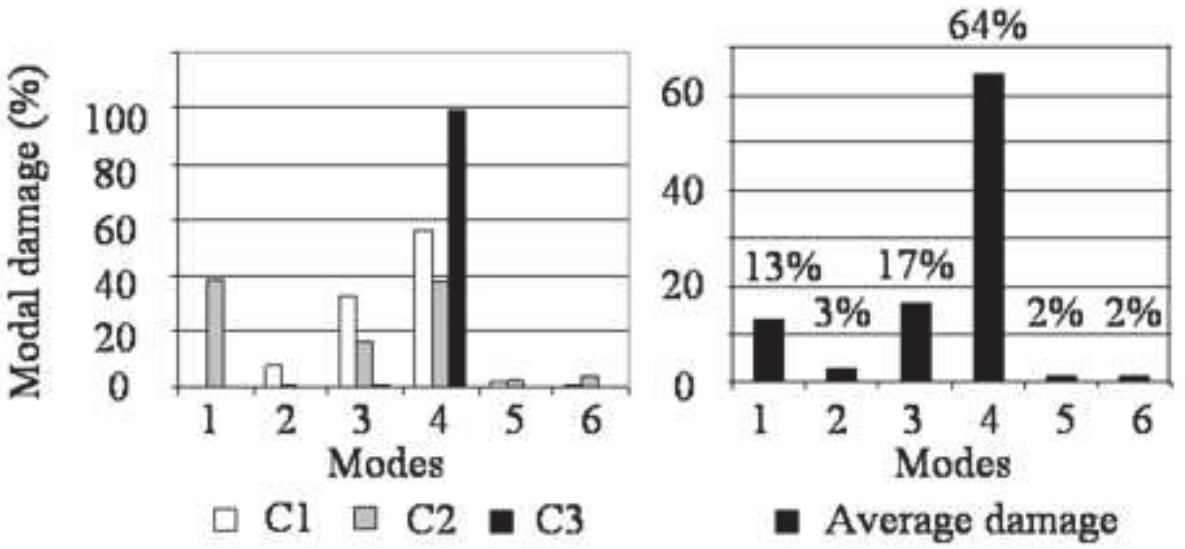

Fig. 4: Component modeling
Click here to download high resolution image

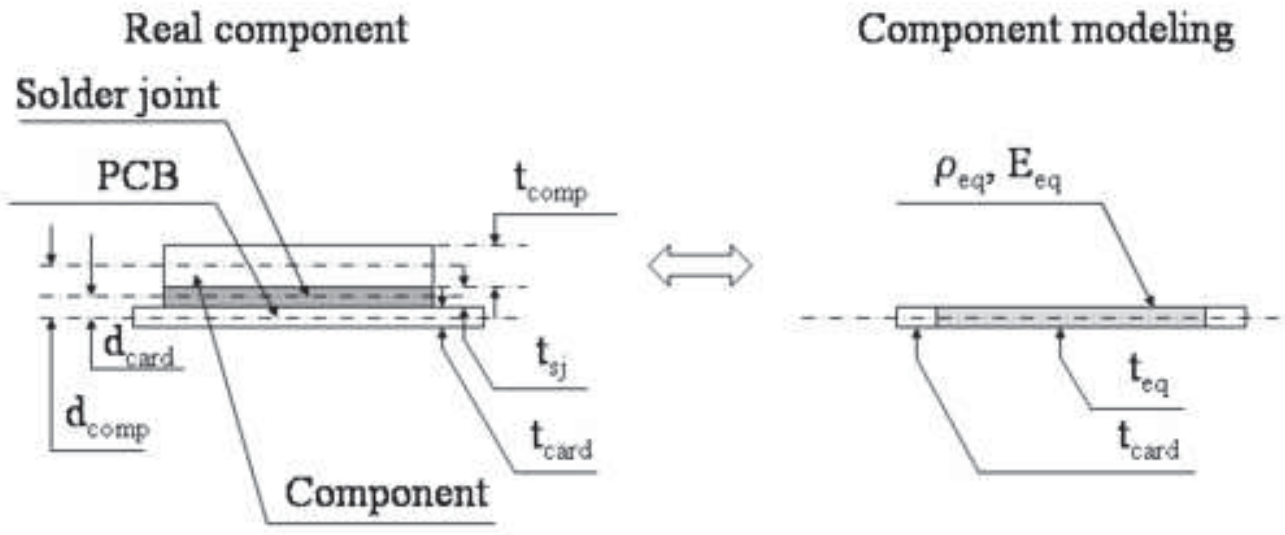

Fig. 5: Optimal location
Click here to download high resolution image

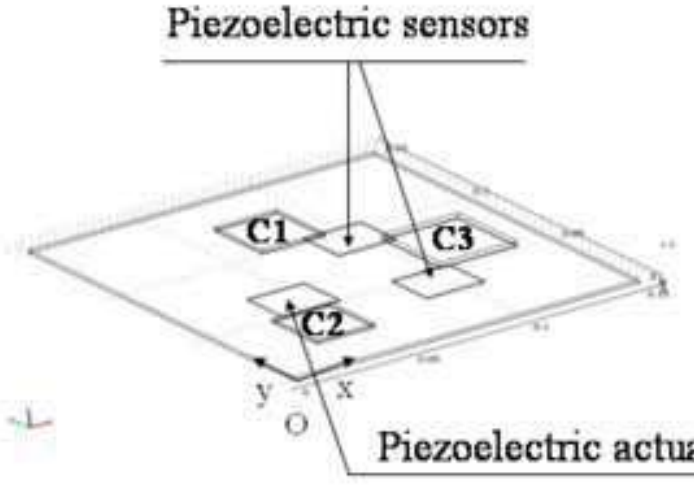

	Location (x,y) (mm)
Actuator	(33,50)
Sensor 1	(83,83)
Sensor 2	(83,33)

Fig. 6: Damage distribution with piezoelectric components
Click here to download high resolution image

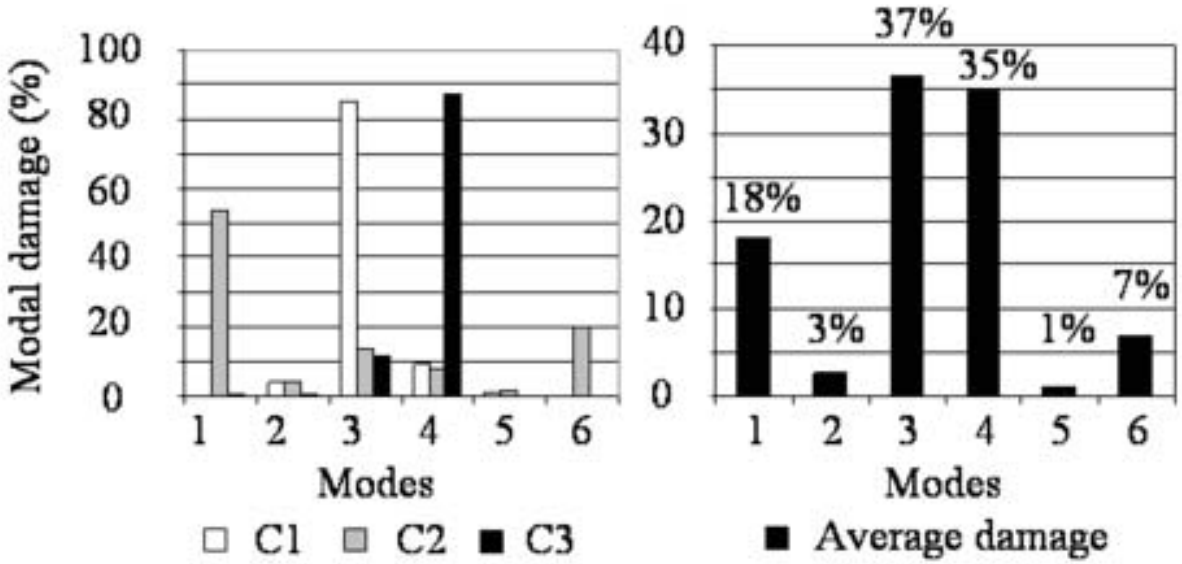

Fig. 7: Numerical uncontrolled and controlled FRF between the ac
Click here to download high resolution image

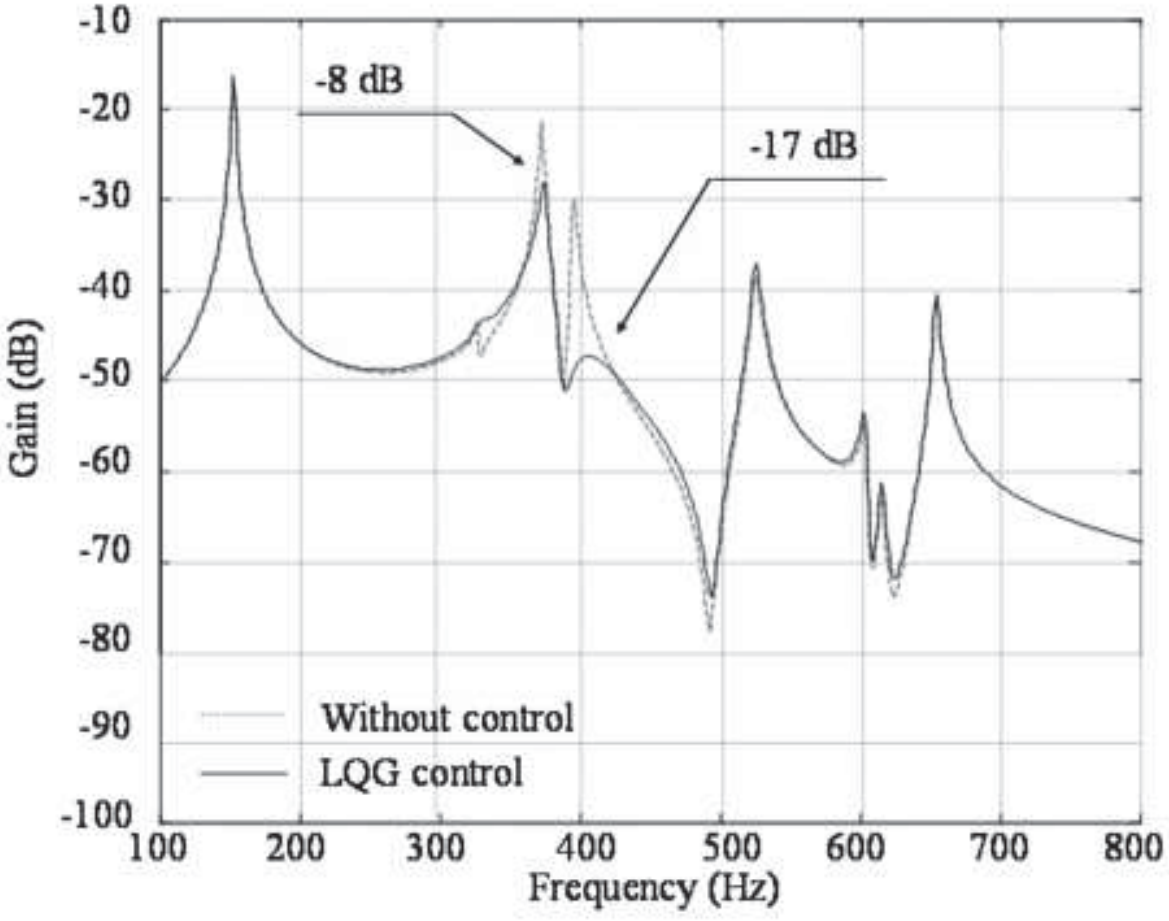

Fig. 8: Numerical control voltage
Click here to download high resolution image

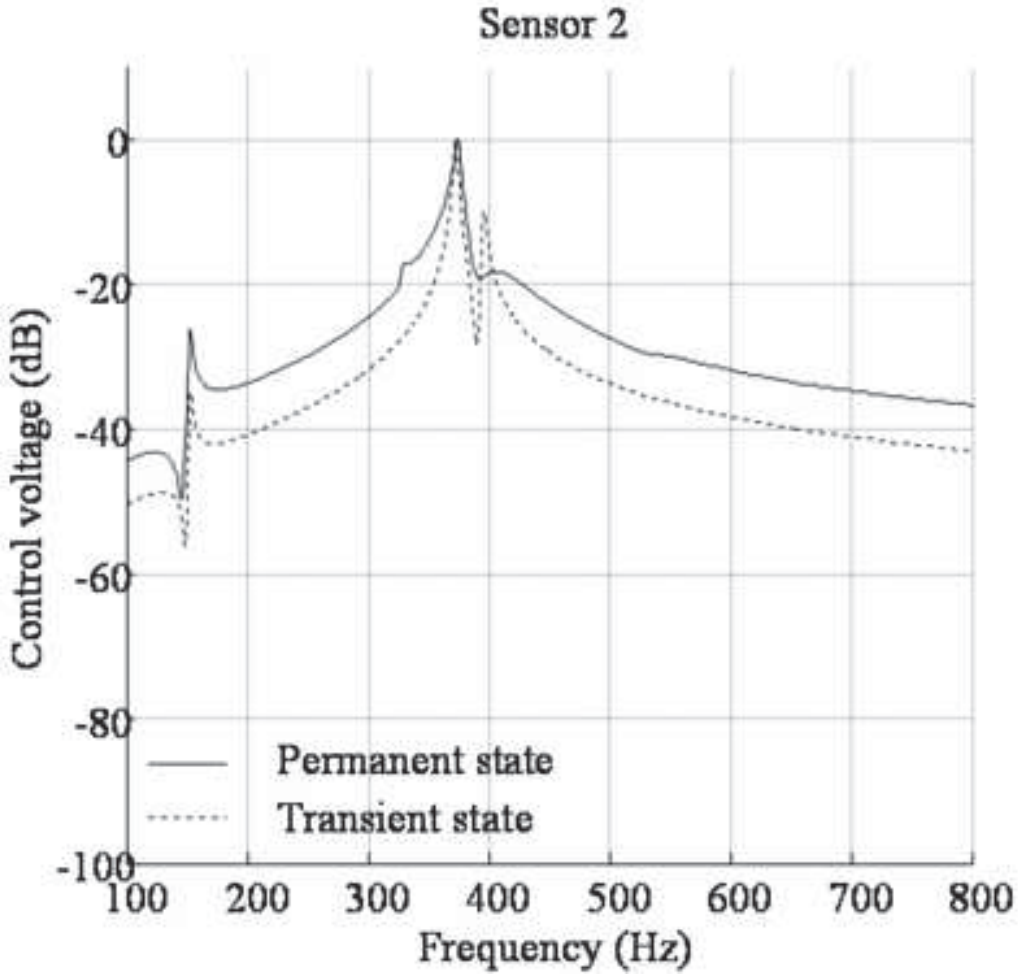

Figure 9 : Experimental set-up
Click here to download high resolution image

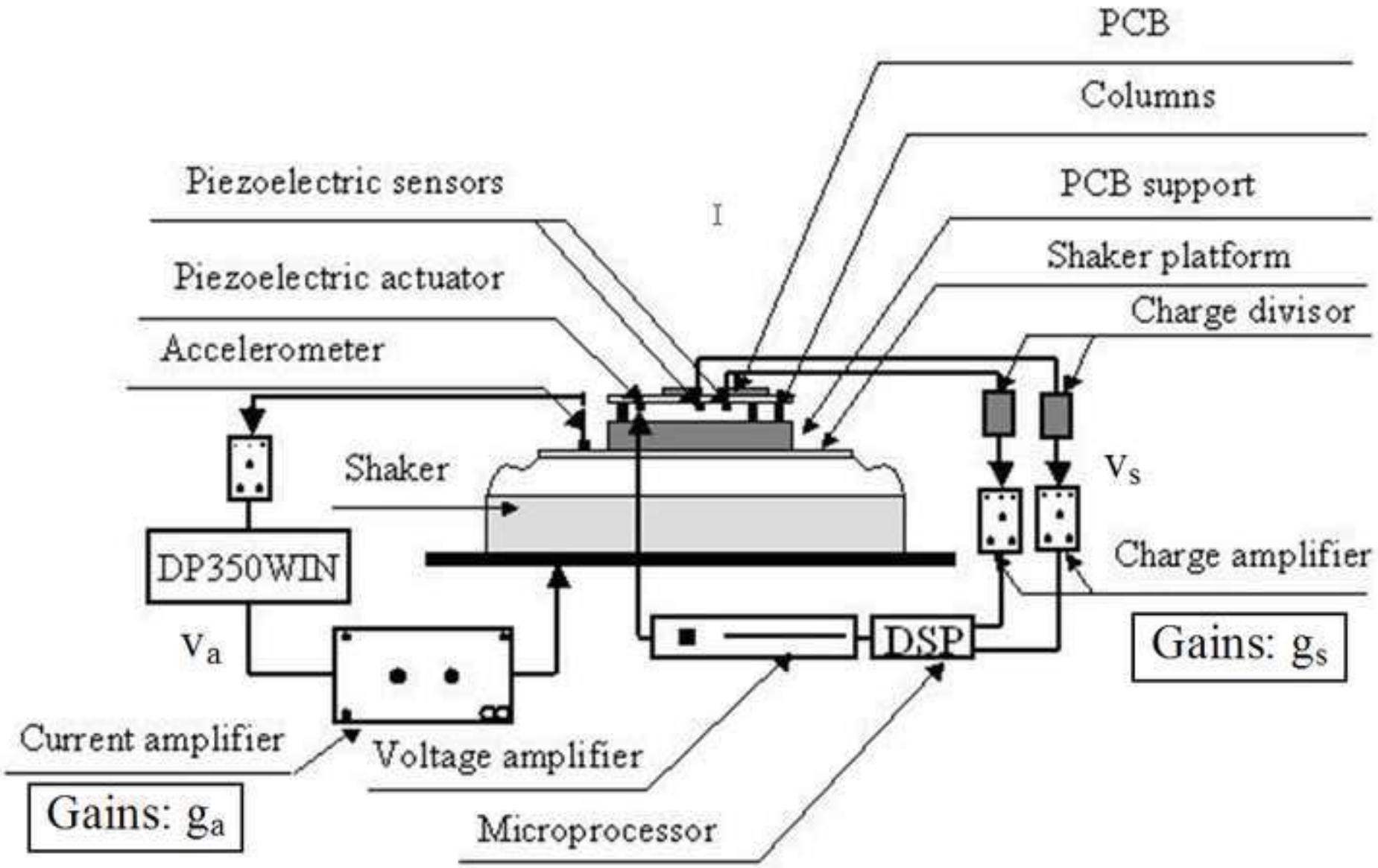

Fig. 10: Experimental uncontrolled and controlled FRF between th
Click here to download high resolution image

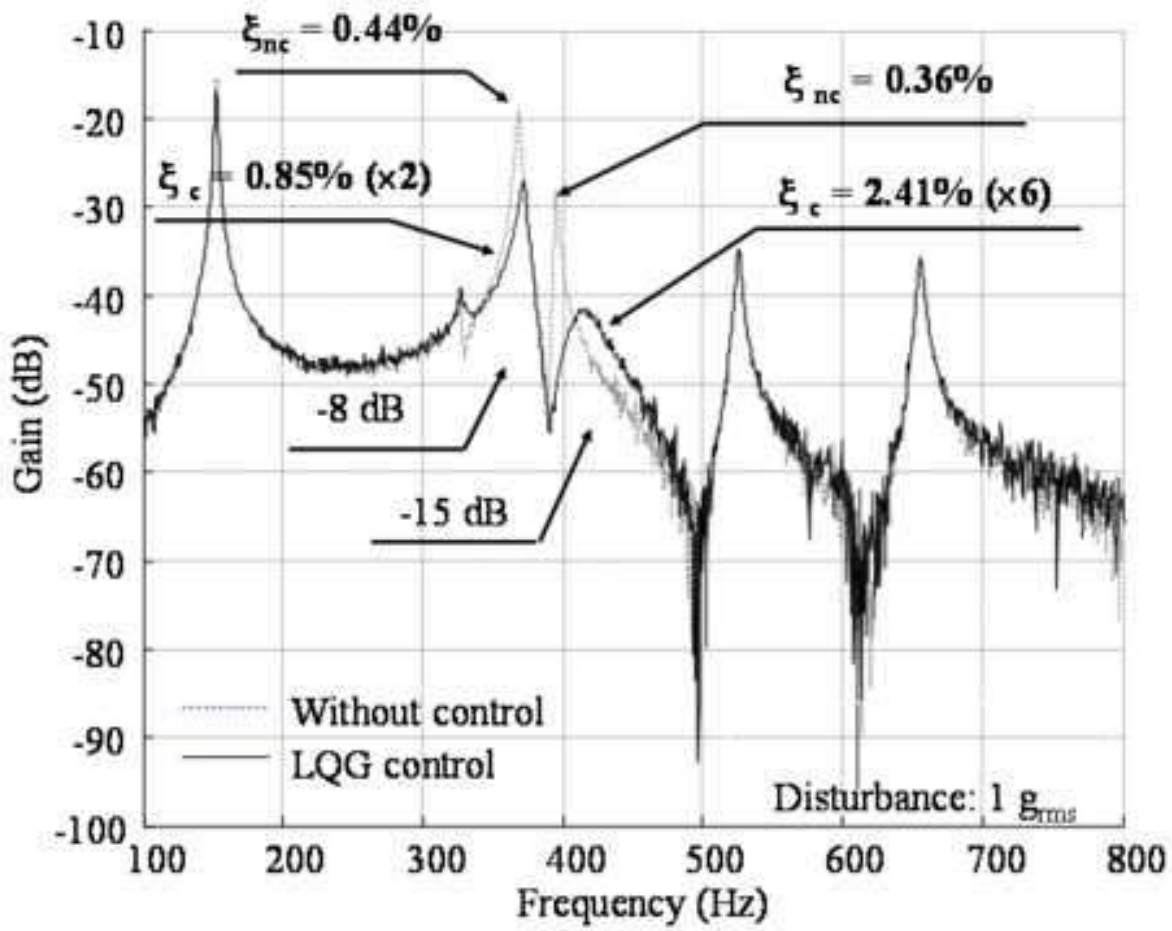

Fig. 11: Modal control voltage for a 1 grms disturbance
Click here to download high resolution image

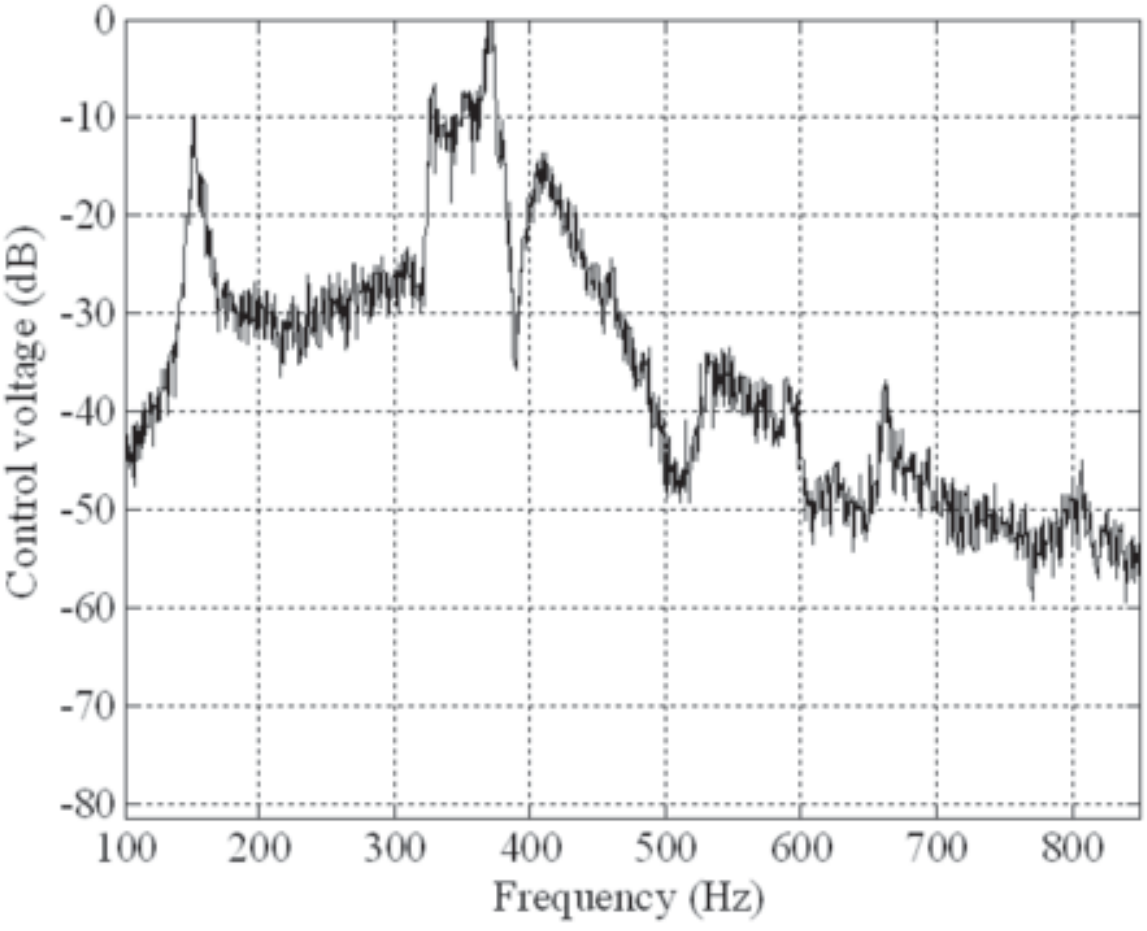

Fig.12: Experimental uncontrolled and controlled FRF between the
Click here to download high resolution image

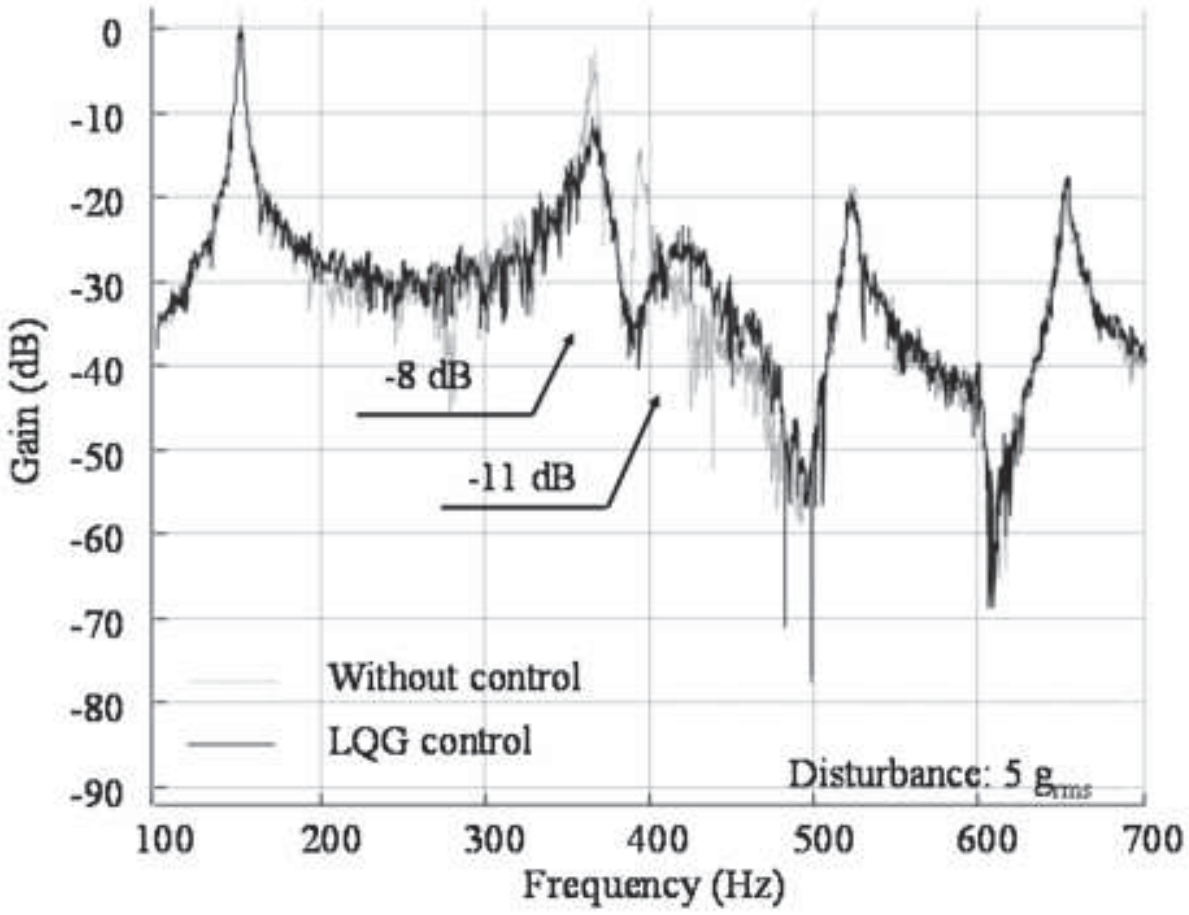

Fig.13: Modal control voltage for a 5 grms disturbance
Click here to download high resolution image

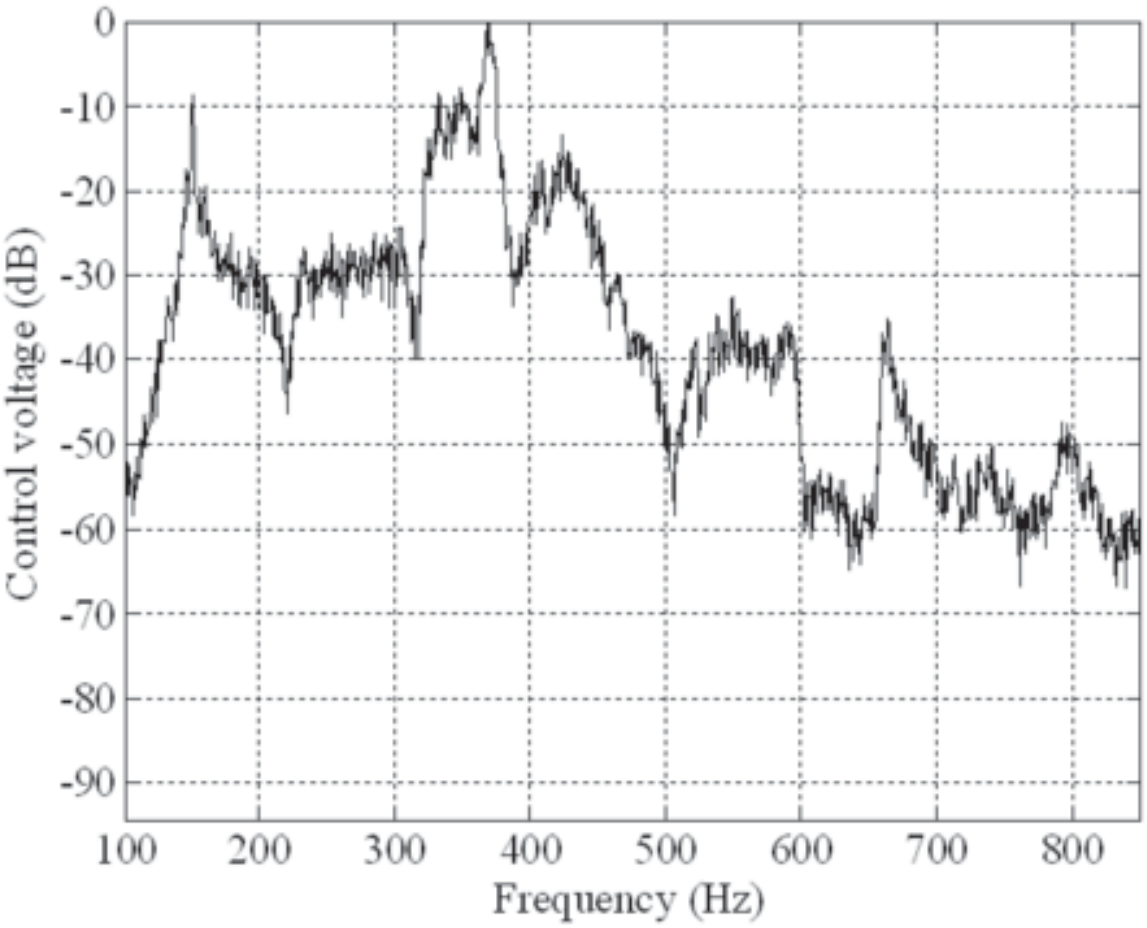

Fig.14: Damage distribution with piezoelectric components and LQ
Click here to download high resolution image

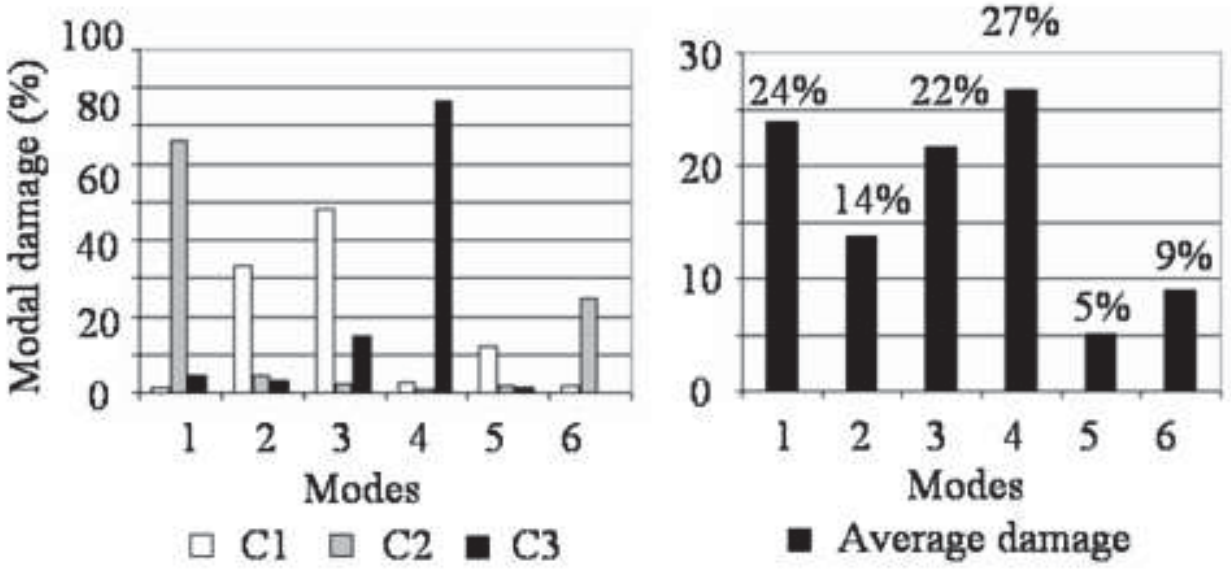

Fig.15: Total damage reduction on the PCB
Click here to download high resolution image

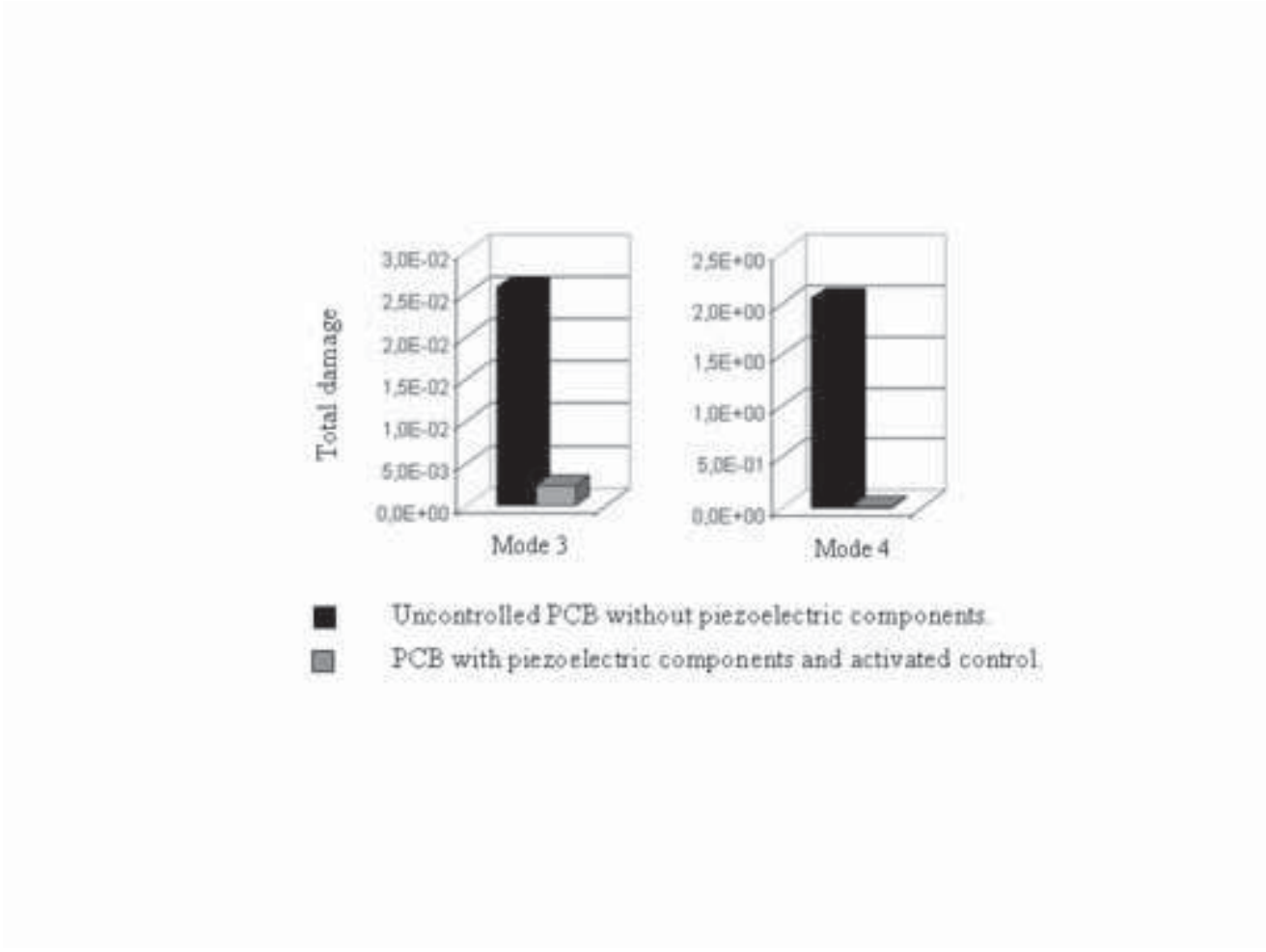

Fig.16: Damage reduction with LQG control calculated with CirVib
Click here to download high resolution image